

Towards an event-based corpuscular model for optical phenomena

H. De Raedt,^a F. Jin^b, and K. Michielsen^b

^a Department of Applied Physics, Zernike Institute for Advanced Materials, University of Groningen, Nijenborgh 4, NL-9747 AG Groningen, The Netherlands

^b Institute for Advanced Simulation, Jülich Supercomputing Centre, Research Centre Jülich, D-52425 Jülich, Germany

ABSTRACT

We discuss an event-based corpuscular model of optical phenomena that does not require the knowledge of the solution of a wave equation of the whole system and reproduces the results of Maxwell's theory through a series of cause-and-effect processes, starting with the emission and ending with the detection of a particle. Event-based models of a single-photon detector and of light propagation through an interface of two dielectrics are used as modular building blocks to give a unified, corpuscular description of many optical phenomena. The approach is illustrated by applications to Wheeler's delayed choice, Einstein-Podolsky-Rosen-Bohm and Hanbury Brown-Twiss experiments.

Keywords: Interference, EPR experiment, Hanbury Brown-Twiss experiment, Event-by-event simulation

1. INTRODUCTION

Interference experiments with light sources^{1,2} and particles such as electrons³⁻⁵ and neutrons⁶⁻⁸ show that the emergence of interference patterns appear as more and more detection events are registered. Identifying a click of a detector with the arrival of a particle, experiments show that the interference pattern is built up gradually, one particle at a time. In some of these experiments, it is highly unlikely that the entities that caused two successive clicks interact with each other.^{1,2,4,6,8} Therefore, it is of interest to enquire why individual entities that do not interact with each other can exhibit the collective behavior that gives rise to the observed interference patterns.

Our approach for solving this problem is to construct an event-by-event simulation model that reproduces the statistical distributions of quantum and Maxwell's theory without solving a wave equation. Our model does not rely on concepts of quantum theory, but provides a logically consistent, cause-and-effect description of phenomena such as interference and entanglement. Although difficult to analyze by traditional methods of theoretical physics, the approach has the virtue that it is easily realized on a digital computer.

For conciseness, this paper will focus on the event-based simulation of experiments with photons. By definition, the emission and detection of a photon are considered to be an event. Likewise, the interaction of a photon with a material constitutes an event. Note that our approach does not model the photon as such. Rather, the photon is viewed as a messenger carrying a message. The creation of a messenger is an event, as are interactions with materials. Absorption and detection of a photon correspond to events that remove the messenger from the system. The simulation algorithm is a collection of simple rules that specify what happens at a particular event. Material is viewed as a processor that responds to an incoming messenger by updating its own internal state and sending out the messenger with a possibly modified message. Thus, the experimental setup is represented as a message-passing system. Crucial thereby is that the messengers never directly communicate with each other: Communication is via the processors representing the material. In such a message passing system, interference patterns appear as the collective result of processing many events, not because there are "interacting waves".^{9,10}

Further author information: (Send correspondence to H. De Raedt)

H. De Raedt : E-mail: h.a.de.raedt@rug.nl

F. Jin: E-mail: F.Jin@fz-juelich.de

K. Michielsen: E-mail: k.michielsen@fz-juelich.de

The Nature of Light: What are Photons? IV, edited by Chandrasekhar Roychoudhuri, Andrei Yu. Khrennikov, Al F. Kracklauer, Proc. of SPIE Vol. 8121, 812103 · © 2011 SPIE
CCC code: 0277-786X/11/\$18 · doi: 10.1117/12.887438

The present paper is not concerned with an interpretation or an extension of quantum theory. The existence of an event-based description of wave phenomena does not affect the validity and applicability of quantum theory or Maxwell's theory but shows that it is possible to give explanations of observed phenomena that do not find a logically consistent, rational explanation within these two theories. We show that quantum optics experiments which are performed in the single-photon regime, that is when detector clicks are being recorded, can be explained

- with a universal event-based corpuscular model,
- without first solving a wave equation.

The event-based corpuscular model (EBCM) that we describe in this paper is universal. It can without modification, be used to explain why photons build up interference patterns, why they can exhibit correlations that cannot be explained within Maxwell's theory and so on. In this sense, the EBCM unifies and extends earlier work.^{11–25} The EBCM gives a cause-and-effect description for every step of the process, starting with the emission and ending with the detection of the photon. By construction, the EBCM satisfies Einstein's criterion of local causality. An appealing feature of the EBCM is that it allows for an explanation of quantum optics experiments in terms of concepts that relate to every-day experience.

2. SIMULATION MODEL

In this section, we give a detailed description of the EBCM of basic optical components, the interface between two media and single-photon detectors. For simplicity of presentation, we consider materials for which the permittivity is real and the permeability is one, that is we consider ideal dielectrics only.

2.1 Messenger and message

A minimal requirement of an EBCM that reproduces the results of Maxwell's theory is that it can mimic the behavior of a plane wave interacting with a material. Therefore, as a start, it makes sense to define the messenger and the message such that there is a one-to-one mapping onto the properties of the plane wave. The EBCM that we introduce in this paper is not a complete event-based model for all electrodynamic phenomena. The focus of this paper is on optics experiments. In accordance with the classical theory of optics,²⁶ for simplicity, we therefore ignore the interaction of electromagnetic radiation with the magnetic degrees of freedom of the materials. It is not difficult to incorporate these interactions in the EBCM: All that is needed is to add more data to the message carried by the messengers and to define the appropriate transformation rules.

The particle is regarded as a messenger, traveling with velocity v in the direction \mathbf{q}/q . Each messenger carries with it two harmonic oscillators that vibrate with frequency f . The length of the vector \mathbf{q} is given by $q = 2\pi f/v$. There are many different, equivalent ways to define the message. As in Maxwell's theory and quantum theory, it is convenient (though not essential) to work with complex-valued vectors, that is with messages represented by two-dimensional unit vectors $\mathbf{y}^T = (e^{i\psi^{(1)}} \sin \xi, e^{i\psi^{(2)}} \cos \xi)$ where $\psi^{(i)} = 2\pi ft + \delta_i$ for $i = 1, 2$. Note that, unlike in the case of waves, there is no $\mathbf{q} \cdot \mathbf{r}$ contribution to $\psi^{(i)}$. The angle ξ determines the relative magnitude of the two components, which we call "polarization" because it is the event-based equivalent of the polarization of a plane electromagnetic wave.²⁶ When a messenger is created, its message needs to be initialized, that is we have to specify the three angles $\psi^{(1)}$, $\psi^{(2)}$, and ξ . This specification depends on the kind of light source we want to simulate. For instance, to simulate a coherent light source, the three angles should be the same for all messengers that are being created.

A messenger with message \mathbf{y} at time t and position \mathbf{r} that travels along the direction \mathbf{q} during a time interval $t' - t$, changes its message according to $\psi^{(i)} \leftarrow \psi^{(i)} + \phi$ for $i = 1, 2$ where $\phi = 2\pi f(t' - t)$. We may view the two-component vectors as the coordinates of two local oscillators, carried along by the messengers. In this pictorial description, the messenger encodes its time-of-flight in these two oscillators. Naively, one might imagine the oscillators tracing out a wavy pattern as they travel through space. However, as there is no relation between the times at which the messengers leave the source, it is impossible to characterize all these traces by a common field that depends on one set of space-time coordinates, as required for a wave theory.

Note that in Maxwell's theory, the energy of the electromagnetic field is encoded in the amplitudes of the wave components. In contrast, in the event-based corpuscular approach, the energy of the electromagnetic field is encoded in the amount of particles that crosses an unit area per unit of time.

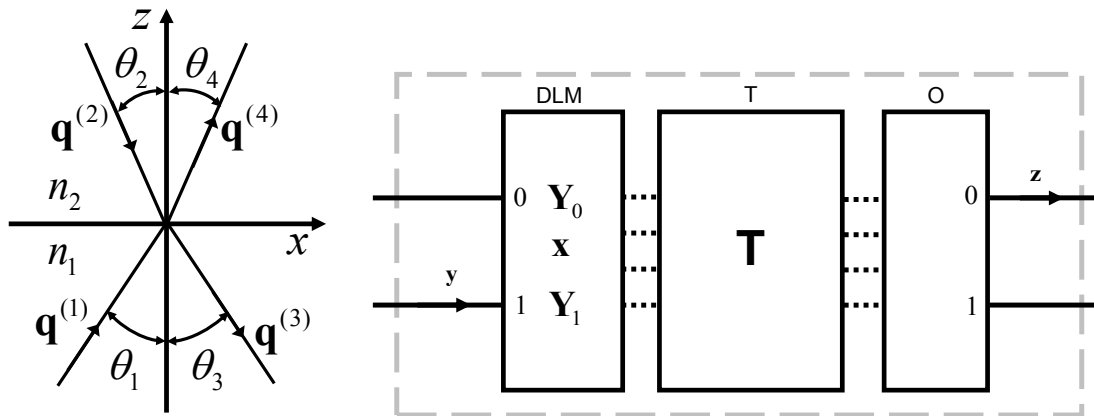


Figure 1. Left: Refraction and reflection at a boundary between two dielectric materials with indices of refraction n_1 and n_2 . The vectors $\mathbf{q}^{(1)}$, $\mathbf{q}^{(2)}$, $\mathbf{q}^{(3)}$, and $\mathbf{q}^{(4)}$ lie in the x - z plane. Right: Universal diagram of a DLM-based processing unit that performs an event-based simulation of optical components. The processing unit consists of three stages: An input stage (DLM), a transformation stage (T) and an output stage (O). The solid lines represent the input and output ports of the device. The presence of a message is indicated by an arrow on the corresponding port line. The dashed lines indicate the data flow within the unit. The transformation matrix \mathbf{T} is optical-component specific.

2.2 Interface between two dielectric media

In Maxwell's theory, assuming incident plane waves from both sides of the interface (see Fig. 1(left)), the directions and amplitudes of the reflected and transmitted plane wave follow from conservation of energy and the continuity of the tangential field components at the boundary, yielding Snell's law and Fresnel's formulas, respectively. Clearly, in an EBCM of refraction and reflection at a dielectric, lossless interface, there can be no loss of particles: An incident particle must either bounce back from or pass through the interface. The conditions on the wave amplitudes in Maxwell's theory translate into conditions on the direction and phases of the two oscillators carried by the reflected or transmitted particle. In the EBCM there are no wave amplitudes, only particle currents. Therefore, continuity is imposed on the particle current.

A processing unit has the generic structure depicted in Fig. 1(right). It consists of an input stage, a deterministic learning machine (DLM), a transformation stage (T), and an output stage (O).¹¹⁻¹⁴ There are two input and two output ports labeled by $k = 0, 1$. Referring to Fig. 1(right), input port $k = 0, 1$ accepts messengers travelling along directions $\mathbf{q}^{(1)}/q^{(1)}$ and $\mathbf{q}^{(2)}/q^{(2)}$, respectively (recall that at any time, only one messenger arrives at either port 0 or 1). Likewise, a messenger leaves in the directions $\mathbf{q}^{(3)}/q^{(3)}$ and $\mathbf{q}^{(4)}/q^{(4)}$ through output port $k = 0, 1$, respectively. For convenience, we choose the coordinate system such that the first oscillator vibrates in the plane that is orthogonal to the plane of incidence (the xz -plane in Fig. 1(left)) while its second oscillator vibrates in the plane that is parallel to the plane of incidence, corresponding to S and P polarized plane waves, respectively.²⁶

2.2.1 Input stage

We represent the arrival of a messenger at port 0 or 1 by the vectors $\mathbf{v} = (1, 0)$ or $\mathbf{v} = (0, 1)$, respectively. The DLM receives a message on either input port 0 or 1, never on both ports simultaneously. The purpose of the DLM is to estimate, without having to store all messages, the relative frequencies with which the messengers arrive on port 0 or (exclusive) 1. The simplest DLM that is capable of performing this task has an internal vector $\mathbf{x} = (x_0, x_1)$, where $x_0 + x_1 = 1$ and $x_k \geq 0$ for all $k = 0, 1$.¹¹ In addition to the internal vector \mathbf{x} , the DLM needs to have two sets of two registers $\mathbf{Y}_k = (Y_{k,1}, Y_{k,2})$ to store the last message \mathbf{y} that arrived at port k . Thus, the DLM has storage for exactly ten real-valued numbers.

Upon receiving a messenger at input port k , the DLM performs the following steps: It copies the elements of message \mathbf{y} in its internal register \mathbf{Y}_k ($\mathbf{Y}_k \leftarrow \mathbf{y}$) while leaving \mathbf{Y}_{1-k} unchanged and replaces its internal vector

according to

$$\mathbf{x} \leftarrow \gamma \mathbf{x} + (1 - \gamma) \mathbf{v}, \quad (1)$$

where $0 \leq \gamma < 1$. Note that each time a messenger arrives at one of the input ports, the DLM replaces the values of the internal vector \mathbf{x} and of the ones in the registers \mathbf{Y}_k by overwriting the old ones. It does not store all the messages, but only two!

2.2.2 Transformation stage

The second stage (T) accepts a message from the input stage, and transforms it into a new message. From the description of the input stage, it is clear that the internal registers \mathbf{Y}_0 and \mathbf{Y}_1 contain the last message that arrived on input port 0 and 1 respectively. First, this data is combined with the data of the internal vector \mathbf{x} , the components of which converge (after many events have been processed) to the relative frequencies with which the messengers arrive on port 0 and 1, respectively. The output message generated by the input stage is

$$\begin{pmatrix} Y'_{0,1} \\ Y'_{1,1} \\ Y'_{0,2} \\ Y'_{1,2} \end{pmatrix} = \begin{pmatrix} x_0^{1/2} & 0 & 0 & 0 \\ 0 & x_1^{1/2} & 0 & 0 \\ 0 & 0 & x_0^{1/2} & 0 \\ 0 & 0 & 0 & x_1^{1/2} \end{pmatrix} \begin{pmatrix} Y_{0,1} \\ Y_{1,1} \\ Y_{0,2} \\ Y_{1,2} \end{pmatrix}, \quad (2)$$

Note that as $x_0 + x_1 = 1$ and $\|\mathbf{Y}_0\| = \|\mathbf{Y}_1\| = 1$, we have $|Y'_{0,1}|^2 + |Y'_{0,2}|^2 + |Y'_{1,1}|^2 + |Y'_{1,2}|^2 = 1$.

Recall that in the EBCM, the number of incoming messengers with message \mathbf{Y}_k represents the energy-density current of the corresponding plane wave, which by construction is proportional to $|\mathbf{Y}_k|^2$. The outgoing energy-density currents are given by

$$\begin{pmatrix} Z_{0,1} \\ Z_{1,1} \\ Z_{0,2} \\ Z_{1,2} \end{pmatrix} = \mathbf{T} \begin{pmatrix} Y'_{0,1} \\ Y'_{1,1} \\ Y'_{0,2} \\ Y'_{1,2} \end{pmatrix}, \quad (3)$$

where the transformation matrix \mathbf{T} is given by

$$\mathbf{T} = \begin{pmatrix} \tilde{r}_S & \tilde{t}_S & 0 & 0 \\ \tilde{t}_S & -\tilde{r}_S & 0 & 0 \\ 0 & 0 & \tilde{r}_P & \tilde{t}_P \\ 0 & 0 & \tilde{t}_P & -\tilde{r}_P \end{pmatrix}, \quad (4)$$

where $\tilde{r}_S = (n_1 \hat{q}^{(1)} - n_2 \hat{q}^{(4)}) / (n_1 \hat{q}^{(1)} + n_2 \hat{q}^{(4)})$, $\tilde{t}_S = 2(n_1 n_2 \hat{q}^{(1)} \hat{q}^{(4)})^{1/2} / (n_1 \hat{q}^{(1)} + n_2 \hat{q}^{(4)})$, $\tilde{r}_P = (n_1 \hat{q}^{(4)} - n_2 \hat{q}^{(1)}) / (n_1 \hat{q}^{(4)} + n_2 \hat{q}^{(1)})$, and $\tilde{t}_P = 2(n_1 n_2 \hat{q}^{(1)} \hat{q}^{(4)})^{1/2} / (n_1 \hat{q}^{(4)} + n_2 \hat{q}^{(1)})$ correspond to messages that represent *S*-polarized and *P*-polarized waves, respectively. To simplify the notation somewhat, we have introduced the symbols $\hat{q}^{(i)} = q_z^{(i)} / q^{(i)} = (-1)^i \cos \theta_i$ for $i = 1, 2, 3, 4$, $n_3 = n_1$ and $n_4 = n_2$. As a result of the choice of the coordinate system, we have $q^{(i)} = ((q_x^{(i)})^2 + (q_z^{(i)})^2)^{1/2}$ for $i = 1, 2, 3, 4$ and conservation of momentum in the *x*-direction implies $q_x^{(1)} = q_x^{(2)} = q_x^{(3)} = q_x^{(4)}$. Hence, the matrix elements in Eq. (4) are completely determined in terms of the incoming message and the properties of the material. Of course, these relations are nothing but Snell's law and the Fresnel equations in disguise.

2.2.3 Output stage

The output stage (O) uses the data provided by the transformation stage (T) to decide on which of the two ports it will send out a messenger (representing a photon). The rule is very simple: We compute $z = |Z_{1,1}|^2 + |Z_{1,2}|^2$ and select the output port \hat{k} by the rule

$$\hat{k} = \Theta(z - r), \quad (5)$$

where $\Theta(\cdot)$ is the unit step function and the $0 \leq r < 1$ is a uniform pseudo-random number (which is different for each messenger processed). The messenger leaves through port \hat{k} carrying the message

$$\mathbf{z} = \frac{1}{\sqrt{|\hat{Z}_{k,1}|^2 + |\hat{Z}_{k,2}|^2}} \begin{pmatrix} \hat{Z}_{k,1} \\ \hat{Z}_{k,2} \end{pmatrix}, \quad (6)$$

which, for reasons of internal consistency, is a unit vector.

2.2.4 Remarks

The internal vector of the DLM can be given physical meaning: It represents the polarization vector of the charge distribution of an atom. The update rule Eq. (1) defines the equation of motion of this vector. In essence, the EBCM is a simplified version of the classical Newtonian model for the response of the polarization of an atom/molecule to the applied electric field,²⁶ with one important difference: It describes the interaction of a single photon with the atom. The update rule Eq. (1) is not the only rule which yields an EBCM that reproduces the results of Maxwell's theory.²⁵ The question of uniqueness of the update rule can only be settled by a new type of experiment that addresses this specific question.²⁷

2.3 Single-photon detectors

Photon detectors, such as a photographic plate or CCD arrays, consist of many identical detection units each having a predefined spatial window in which they can detect photons. In what follows, each of these identical detection units will be referred to as a detector. By construction, these detector units operate completely independently from and also do not communicate with each other.

In essence, a detector consists of material that absorbs light. The electric charges that result from the absorption process are then amplified, chemically in the case of a photographic plate or electronically in the case of photo-diodes or photomultipliers. In the case of photomultipliers or photo-diodes, once a photon has been absorbed (and its energy "dissipated" in the detector material) an amplification mechanism (which requires external power/energy) generates an electric current (provided by an external current source).^{28,29} The resulting signal is compared with a threshold that is set by the experimenter and the photon is said to have been detected if the signal exceeds this threshold.^{28,29} In the case of photographic plates, the chemical process that occurs when photons are absorbed and the subsequent chemical reactions that renders visible the image serve similar purposes.

In the wave-mechanical picture, the interaction between the incident electric field \mathbf{E} and the material takes the form $\mathbf{P} \cdot \mathbf{E}$, where \mathbf{P} is the polarization vector of the material.²⁶ Treating this interaction in first-order perturbation theory, the detection probability reads $P_{\text{detection}}(t) = \int_0^t \int_0^t \langle \langle \mathbf{E}^T(t') \cdot \mathbf{K}(t' - t'') \cdot \mathbf{E}(t'') \rangle \rangle dt' dt''$ where $\mathbf{K}(t' - t'')$ is a memory kernel depending on the material only and $\langle \langle \cdot \rangle \rangle$ denotes the average with respect to the initial state of the electric field.^{28,30} Both the constitutive equation²⁶ $\mathbf{P}(\omega) = \chi(\omega)\mathbf{E}(\omega)$ as well as the expression for $P_{\text{detection}}(t)$ show that the detection process involves some kind of memory, as is most evident in the case of photographic films before development. It is important to take note of the fact that for the integration over t' and t'' to yield physically meaningful results, within the context of a wave theory, the interaction interval $[0, t]$ should extend over many periods of the wave.²⁶

An event-based model for the detector clicks cannot be "derived" from quantum theory simply because quantum theory predicts the frequencies of the clicks has nothing to say about individual events themselves.³¹ Therefore, any model for the detector that operates on the level of single events must necessarily appear as "ad hoc" from the viewpoint of quantum theory. The event-based detector model that we describe in this paper should not be regarded as realistic models for say, a photomultiplier or a photographic plate and the chemical process that renders the image. It is perhaps the simplest event-based model that captures the salient features of ideal (i.e. 100% efficient) single-photon detectors without making reference to the solution of a wave equation or quantum theory.

The schematic diagram depicted in Fig. 2 shows that the processing unit acting as a single-photon detector has the same structure as the processing unit for the interface, see Fig. 1, except that the number of input ports, denoted by $N_p = K + 1$, may be larger than two. This extension is necessary because a detector should be able to process messengers that come from many different directions.

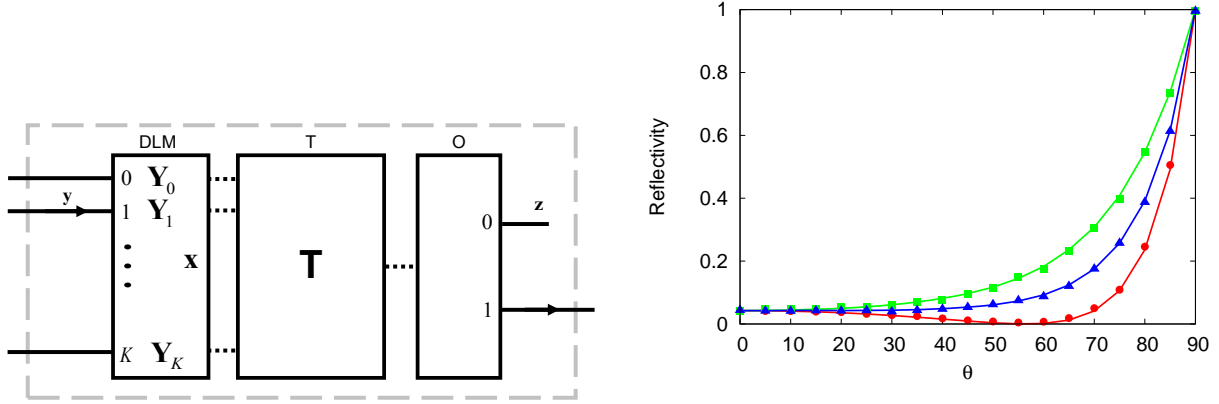


Figure 2. Left: Diagram of the event-based detector model. The dashed lines indicate the data flow within the processing unit. Right: EBCM simulation results (markers) for the reflectivity of an interface between vacuum ($n_1 = 1$) and glass ($n_2 = 1.52$) as a function of the angle of incidence of the incoming particles (see also Fig.1.12 of Ref.²⁶). The solid lines are the exact results of Maxwell's theory.²⁶ Green markers and lines: $\xi = 0$ (S -polarization); Blue markers and lines: $\xi = \pi/4$ ($S+P$ polarization); Red markers and lines: $\xi = \pi/2$ (P -polarization). Simulation parameters: 10^4 events per marker, $\gamma = \hat{\gamma} = 0.99$ and $N_p = 1$.

2.3.1 Input stage

Representing the arrival of a messenger at port $0 \leq k \leq K$ by the vector $\mathbf{v} = (v_0, \dots, v_K)^T$ with $v_i = \delta_{i,k}$ the internal vector is updated according to the rule

$$\mathbf{x} \leftarrow \hat{\gamma}\mathbf{x} + (1 - \hat{\gamma})\mathbf{v}, \quad (7)$$

where $\mathbf{x} = (x_0, \dots, x_K)^T$, $\sum_{k=0}^K x_k = 1$, and $0 \leq \hat{\gamma} < 1$. The elements of the incoming message \mathbf{y} are written in internal register \mathbf{Y}_k ($\mathbf{Y}_k \leftarrow \mathbf{y}$) while all the other \mathbf{Y}_i ($i \neq k$) registers remain unchanged. Thus, each time a messenger arrives at one of the input ports, say k , the DLM updates all the elements of the internal vector \mathbf{x} , overwrites the data in the register \mathbf{Y}_k while the content of all other \mathbf{Y} registers remains the same.

2.3.2 Transformation stage

The output message generated by the transformation stage is

$$\mathbf{T} = \mathbf{x} \cdot \mathbf{Y} = \sum_{k=0}^K x_k \mathbf{Y}_k, \quad (8)$$

which is a complex-valued two-component vector, similar to a message \mathbf{y} .

2.3.3 Output stage

As in the event-based model for the interface, the output stage (O) generates a binary output signal $\hat{k} = 0, 1$ but now the output message does not represent a photon: It represents a “no click” or “click” if $\hat{k} = 0$ or $\hat{k} = 1$, respectively. To implement this functionality, we define (compare with Eq. (5) which is essentially the same)

$$\hat{k} = \Theta(|\mathbf{T}|^2 - r), \quad (9)$$

where $\Theta(\cdot)$ is the unit step function and $0 \leq r < 1$ are uniform pseudo-random numbers (which are different for each event). The parameter $0 \leq \hat{\gamma} < 1$ can be used to control the operational mode of the unit. From Eq. (9) it follows that the frequency of $\hat{k} = 1$ events depends on the length of the internal vector \mathbf{T} .

Note that in contrast to experiment, in a simulation, we could register both the $\hat{k} = 0$ and $\hat{k} = 1$ events. Then the sum of the $\hat{k} = 0$ and $\hat{k} = 1$ events is equal to the number of input messages. In real experiments,

only $k = 1$ events are taken as evidence that a photon has been detected. Therefore, we define the total detector count by

$$N_{\text{count}} = \sum_{l=1}^K \hat{k}_l, \quad (10)$$

where K is the number of messages received and l labels the events. In words, N_{count} is the total number of one's generated by the detector unit.

2.3.4 Detection efficiency

In general, the detection efficiency is defined as the overall probability of registering a count if a photon arrives at the detector.²⁹ One method to measure the detection efficiency is to use a single-photon point source, placed far away from a single detector.²⁹ In an EBCM of such an experiment, all the messengers that reach the detector will approximately have the same direction, implying that these messengers arrive at this detector at the same input port, say k . Under these circumstances, x_k converges exponentially fast to one. Hence, after receiving a few photons, the detector clicks every time a photon arrives. Thus, the detection efficiency, as defined for real detectors, of the event-based detector model is very close to 100%. Comparing the number of ad hoc assumptions and unknown functions that enter typical quantum theory treatments of photon detectors²⁸ with the two parameters $\hat{\gamma}$ and N_p of the event-based detector model, the latter has the virtue of being extremely simple while providing a description of the detection process at the level of detail, the single events, which is outside the scope of quantum theory.

3. MODEL VALIDATION

We validate the EBCM by simulating some very basic optical experiments such as reflection and refraction by a boundary between two dielectric materials and by a plane parallel plate and the interference of two light beams. As an example, in Fig. 2(right), we compare EBCM simulation results with the predictions of Maxwell's theory for the reflectivity of an interface between vacuum and glass as a function of the angle of incidence.²⁶ It is clear that there is excellent agreement, even though the number of emitted events is small compared to the number of photons used in typical optics experiments. Obviously, the EBCM passes this test. Results of other simple tests, such as interference by a parallel plate are given elsewhere.²⁵

4. OPTICAL COMPONENTS

The EBCM of optical components such as wave plates and beam splitters can be constructed by connecting several units that simulate the interfaces (with suitable parameters) of these components.³² From a simulation point of view, such a construction is both inefficient and unnecessary. Having shown that two connected EBCM's of an interface reproduce the result of a plane parallel plate, it is legitimate to replace the two interfaces by one "lumped" EBCM that simulates a beam splitter for instance.³² The full specification of the event-based processors that acts as (polarizing) beam splitters, wave plates etc. can be found in Ref.²⁵

5. SINGLE-PHOTON QUANTUM OPTICS EXPERIMENTS

In the EBCM approach, the processing units that simulate the optical components are connected in such a way that the simulation setup is an exact one-to-one copy of the laboratory experiment. The source sends messengers one-by-one but at all times, there is at most one message being routed through the network of processing units. Only after a detector has processed the message, the source is allowed to create a new messenger. This procedure guarantees that the simulation process trivially satisfies Einstein's criterion of local causality. The quantum optics experiments that we discuss in this paper have been chosen to illustrate that fairly complicated experiments can be simulated without any change to the EBCM. Additional EBCM simulations are reported elsewhere.²⁵

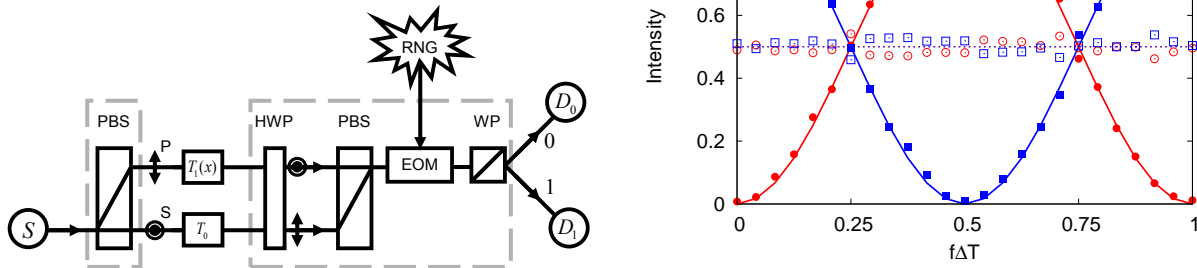


Figure 3. Left: Schematic diagram of the experimental setup for Wheeler's delayed-choice experiment with single photons.³⁴ PBS: Polarizing beam splitter; HWP: Half-wave plate; EOM: Electro-optic modulator; RNG: Random number generator; WP: Wollaston prism (= PBS); D_0 , D_1 : Detectors. The EBCM replaces the physical devices by the corresponding message-processing units. Right: EBCM simulation results (markers) for the Wheeler delayed-choice experiment depicted in Fig. 3. The number of particles registered by detectors D_0 and D_1 divided by the total count of detected particles, as a function of the difference $\Delta T = (T_0 - T_1(x))$ between the time-of-flight in the lower and upper arm of the interferometer, respectively. In the simulation, the frequency f of the light appears as scale factor in $f\Delta T$ only and can therefore be taken as one. Open circles: Intensity measured by D_0 for $\theta_{\text{EOM}} = 0$ ($r_n = 0$); Open squares: Intensity measured by D_1 for $\theta_{\text{EOM}} = 0$; Closed circles: Intensity measured by D_0 for $\theta_{\text{EOM}} = \pi/4$ ($r_n = 1$); Closed squares: Intensity measured by D_1 for $\theta_{\text{EOM}} = \pi/4$; Dashed line: Intensities measured by D_0 and D_1 as obtained from Maxwell's theory for $\theta_{\text{EOM}} = 0$; Solid red (blue) line: Intensity measured by D_0 (D_1) as obtained from Maxwell's theory for $\theta_{\text{EOM}} = \pi/4$. Simulation parameters: 2600 emitted events per pair of open/closed markers, $\gamma = \hat{\gamma} = 0.99$ and $N_p = 1$. The actual counts (= $1300 \times$ intensities) are in good quantitative agreement with the experimental results reported in Ref.³⁴

5.1 Wheeler's delayed choice experiment

In 1978, Wheeler proposed a gedanken experiment,³³ a variation on Young's double slit experiment, in which the decision to observe wave or particle behavior is made after the photon has passed the slits. The pictorial description of this experiment defies common sense: The behavior of the photon in the past is said to be changing from a particle to a wave or vice versa.

In an experimental realization of Wheeler's delayed choice experiment, Jacques *et al.*³⁴ send linearly polarized single photons through a polarizing beam splitter (PBS) that together with a second, movable PBS forms an interferometer (see Fig. 3). Moving the second PBS induces a time-delay in one of the arms of the interferometer,³⁴ symbolically represented by $T_1(x)$ in Fig. 3. The electro-optic modulator (EOM) performs the same function as a half-wave plate (HWP). Changing the electrical potential applied to the EOM, changes the rotation angle that mixes the two polarizations. In the experiment,³⁴ the random number generator RNG generates a sequence of binary random numbers $r_n = 0, 1$. The output of RNG is used to control the potential applied to the EOM. If $r_n = 0$, the rotation angle $\theta_{\text{EOM}} = 0$ and if $r_n = 1$, $\theta_{\text{EOM}} = \pi/8$. In the former case, there can be no interference: There is no mixing of S - and P -polarized light. In the latter case, interference can occur and we expect an interference pattern that is the same as the one of a Mach-Zehnder interferometer (MZI). Detector D_0 (D_1) counts the events generated at port 0 (1) of the Wollaston prism (WP). During a run of N events, the algorithm generates the data set

$$\Gamma = \{d_n, r_n | n = 1, \dots, N; f\Delta T\}, \quad (11)$$

where $d_n = 0$ (1) indicates that detector D_0 (D_1) fired and $r_n = 0, 1$ is a binary pseudo-random number that is chosen after the n th message has passed the first PBS.

We simulate the Wheeler delayed-choice experiment of Fig. 3 by connecting the various EBCM of the optical components in exactly the same manner as in Fig. 3. The simulation generates the data set Γ just like in the experiment^{34,35} and is analyzed in the same manner. The EBCM simulation results presented in Fig. 3 show that there is excellent agreement between the event-based simulation data and the predictions of wave theory.

In the classical, locally causal EBCM, there is no need to resort to concepts such as particle-wave duality and the mysteries of delayed-choice to give a rational explanation of the observed phenomena. In the simulation we can always track the particles, independent of $r_n = 0, 1$. These particles always have full which-way information, never directly communicate with each other, arrive one by one at a detector but nevertheless build up an interference pattern at the detector if $r_n = 1$. Thus, the EBCM of Wheeler's delayed-choice experiment provides a unified particle-only description of both cases $r_n = 0, 1$ that does not defy common sense.

6. EINSTEIN-PODOLSKY-ROSEN-BOHM EXPERIMENT

In this section, we simply use (without any modification) the EBCMs for the optical components that are present in the laboratory experiment and analyze the simulation data in exactly the same manner as the experimental data for this experiment has been analyzed.³⁶ The resulting EBCM for the whole EPRB experiment is substantially more complicated than our event-based simulation models that reproduce the result of quantum theory for the singlet state and product state.^{15-18,21} The difference is that in our earlier work we adopted the tradition in this particular subfield to use simplified mathematical models for the optical components that, when re-used for different optics experiments, would fail to reproduce the results of these experiments. The EBCM simulation model used in the present work employs models for the optical components that work (unmodified) for all quantum optics experiments.

In Fig. 4, we show a schematic diagram of an EPRB experiment with photons (see also Fig. 2 in Ref.³⁶). The source emits pairs of photons. Each photon of a pair travels to an observation station in which it is manipulated and detected. The two stations are assumed to be identical. They are separated spatially and temporally, preventing the observation at station 1 (2) to have a causal effect on the data registered at station 2 (1).³⁶ As the photon arrives at station $i = 1, 2$, it passes through an EOM that rotates the polarization of the photon by an angle depending on the voltage applied to the modulator. These voltages are controlled by two independent binary random number generators. A PBS sends the photon to one of the two detectors. The station's clock assigns a time-tag to each generated signal. We consider two different experiments, one in which the source emits photons with opposite but otherwise unpredictable polarization and those with a source emitting photons with fixed polarization.

The quantum theoretical description of the EPRB experiment with photons exploits the fact that the two-dimensional vector space spanned by two orthogonal polarization vectors is isomorphic to the vector space of spin-1/2 particles. An EBCM simulation should reproduce the predictions of quantum theory for the single and two-particle averages for a quantum system of two spin-1/2 particles in the singlet state and a product state. The EBCM of the EPRB experiment trivially satisfies Einsteins criteria of local causality, does not rely on any concept of quantum theory and, as will be shown below, reproduces the results of quantum theory for both types of experiments. Recall that the EBCM of the detector mimics a detector with 100% detection efficiency.

In the simulation, the firing of a detector is regarded as an event. At the n th event, the data recorded on a hard disk at station $i = 1, 2$ consists of $x_{n,i} = \pm 1$, specifying which of the two detectors fired, the time tag $t_{n,i}$ indicating the time at which a detector fired, and the two-dimensional unit vector $\alpha_{n,i}$ that represents the rotation of the polarization by the EOM at the time of detection. Hence, the set of data collected at station $i = 1, 2$ during a run of N events may be written as

$$\Upsilon_i = \{x_{n,i} = \pm 1, t_{n,i}, \alpha_{n,i} | n = 1, \dots, N\}. \quad (12)$$

In the (computer) experiment, the data $\{\Upsilon_1, \Upsilon_2\}$ may be analyzed long after the data has been collected.³⁶ Coincidences are identified by comparing the time differences $\{t_{n,1} - t_{n,2} | n = 1, \dots, N\}$ with a time window³⁶ W . Introducing the symbol \sum' to indicate that the sum has to be taken over all events that satisfy $\alpha_i = \alpha_{n,i}$ for $i = 1, 2$, for each pair of directions α_1 and α_2 of the EOMs, the number of coincidences $C_{xy} \equiv C_{xy}(\alpha_1, \alpha_2)$ between detectors $D_{x,1}$ ($x = \pm 1$) at station 1 and detectors $D_{y,2}$ ($y = \pm 1$) at station 2 is given by

$$C_{xy} = \sum_{n=1}^N \delta_{x,x_{n,1}} \delta_{y,x_{n,2}} \Theta(W - |t_{n,1} - t_{n,2}|), \quad (13)$$

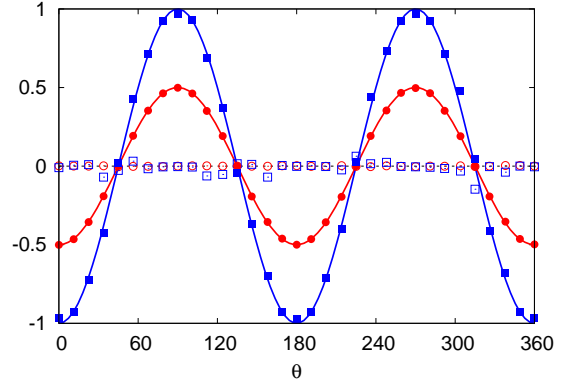
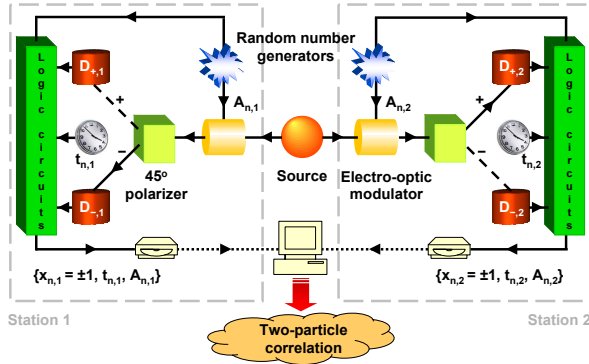


Figure 4. Left: Schematic diagram of an EPRB experiment with photons.³⁶ Right: Computer simulation data and quantum theoretical results for the single-particle and two-particle averages of the EPRB experiment depicted in Fig. 4 as a function of $\theta = \alpha_1 - \alpha_2$. The source emits particles with opposite polarization, uniformly distributed over the unit circle. Open circles and squares: Eq. (14) and (15), respectively; Closed squares: Eq. (16); Bullets: Eq. (16) for $W = T_{\text{EPRB}}$, that is by ignoring the time-tag data; Blue solid line: $\bar{E}_{12}(\alpha_1, \alpha_2) = -\cos 2\theta$; Red solid line: $-2^{-1} \cos 2\theta$. Simulation parameters: 3×10^5 pairs, $T_{\text{EPRB}} = 1000$, $W = 1$, $d = 4$, $\gamma = \hat{\gamma} = 0.99$ and $N_p = 1$. Note that the total number of pairs emitted by the source is about the same as the number of photons per station detected in the experiment reported in Ref.³⁶ (experimental data set called longdist35).

where $\Theta(t)$ is the Heaviside step function. The averages of the single-particle counts are defined by

$$E_1(\alpha_1, \alpha_2) = \frac{C_{++} - C_{--} + C_{+-} - C_{-+}}{C_{++} + C_{--} + C_{+-} + C_{-+}}, \quad (14)$$

and

$$E_2(\alpha_1, \alpha_2) = \frac{C_{++} - C_{--} - C_{+-} + C_{-+}}{C_{++} + C_{--} + C_{+-} + C_{-+}}, \quad (15)$$

where the denominator is the sum of all coincidences. The correlation of two dichotomic variables x and y is defined as

$$E_{12}(\alpha_1, \alpha_2) = \frac{C_{++} + C_{--} - C_{+-} - C_{-+}}{C_{++} + C_{--} + C_{+-} + C_{-+}}. \quad (16)$$

In general, the values for the average single-particle counts $E_1(\alpha_1, \alpha_2)$ and $E_2(\alpha_1, \alpha_2)$, the two-particle averages $E(\alpha_1, \alpha_2)$, and the total number of the coincidences $C(\alpha_1, \alpha_2) = \sum_{x,y=\pm 1} C_{xy}(\alpha_1, \alpha_2)$, not only depend on the directions α_1 and α_2 but also on the time window W used to identify the coincidences.

6.1 Time-tag model

From Eq. (12), it is clear that a model that aims to describe real EPRB experiments should incorporate a mechanism to produce the time tags $t_{n,1}$ and $t_{n,2}$.

To the best of our knowledge, A. Fine was the first to point out that what he called synchronization models, essentially implementing the time-coincidence window employed in laboratory EPRB experiments, may yield the quantum correlation of the quantum model of the EPRB.³⁷ A concrete model of this kind was proposed by S. Pascazio who showed that his model approximately reproduces the correlation of the singlet state³⁸ with an accuracy that seems far beyond what is experimentally accessible to date.

Following our earlier work,¹⁵⁻¹⁸ we assume that as a particle passes through the EOM, it experiences a time delay. This is a very reasonable assumption as EOMs are in fact used as retarders in optical communication systems. For simplicity, the time delay $t_{n,i}$ is assumed to be distributed uniformly over the interval $[0, T]$. From our earlier work we know that the choice $T = T_{\text{EPRB}} \sin^{2d} 2(\xi_n - \alpha_{n,i})$ rigorously reproduces the results of quantum theory for the EPRB experiment if $d = 4$ and $W \ll T_{\text{EPRB}}$.¹⁵⁻¹⁸ Therefore, we adopt this time-tag model in the present paper.

6.2 Simulation results

The EBCM generates the data set Eq. (12), just as experiment does.³⁶ We choose the coincidence window W and compute the coincidences, single-spin and two-spin averages according to the Eqs. (13)–(16). The simulation results for the two experiments in which the source emits fully correlated particles are presented in Figs. 4. The fully classical, locally causal EBCM reproduces the results of quantum theory for both the singlet state and the product state, even though the detectors have 100% detection efficiency.²⁵

6.3 Remarks

The simulation results presented in Fig. 4 provide unambiguous evidence that Bell's no-go theorem is of very limited value: This theorem applies to a marginal class of classical models that do not account for the presence of the (narrow) time-coincidence window in the real experiment.²⁵

7. HANBURY BROWN-TWISS EXPERIMENT

Hanbury Brown-Twiss experiment (HBT) experiments³⁹ measure the correlation of light intensities originating from two different, uncorrelated sources. HBT showed that under conditions for which the usual two-beam interference fringes measured by each of the two detectors vanish, the correlated intensities of the two detectors can still show interference fringes. When a HBT experiment is performed with detectors operating in the single-photon-detection regime, the observation of the fringes in the correlated detector intensities is attributed to the wave-particle duality of the beam.^{40–42}

Conceptually, the HBT experiment, a schematic diagram being shown in Fig. 5(left), can be viewed as a two-beam interference experiment with two detectors. Assume that source S_m ($m = 0, 1$) emits coherent light of frequency f and produces a wave with amplitude $A_m e^{i\phi_m}$ (A_m and ϕ_m real). For simplicity of presentation, we assume that $A_0 = A_1 = A$. According to Maxwell's theory, the total wave amplitude B_n on detector n is

$$B_n = A \left(e^{i(\phi_0 + 2\pi f T_{0,n})} + e^{i(\phi_1 + 2\pi f T_{1,n})} \right), \quad (17)$$

where the time-of-flight for each of the four possible paths from source S_m to detector D_n is denoted by $T_{m,n}$ where $m, n = 0, 1$. The light intensity $I_n = |B_n|^2$ on detector D_n is given by

$$I_n = 2A^2 \{1 + \cos[\phi_0 - \phi_1 + 2\pi f(T_{0,n} - T_{1,n})]\}. \quad (18)$$

If the phase difference $\phi_0 - \phi_1$ in Eq. (18) is fixed, the usual two-beam (first-order) interference fringes are observed. The essence of the HBT experiment is that if the phase difference $\phi_0 - \phi_1$ is a random variable (uniformly distributed over the interval $[0, 2\pi[$) as a function of observation time, these first-order interference fringes vanish because $\langle I_n \rangle = 2A^2$ (in this section, $\langle \cdot \rangle$ denotes the average over the variables ϕ_0 and ϕ_1). However, the average of the product of the intensities is given by

$$\langle I_0 I_1 \rangle = 4A^4 \left(1 + \frac{1}{2} \cos 2\pi f \Delta T \right), \quad (19)$$

where $\Delta T = (T_{0,0} - T_{1,0}) - (T_{0,1} - T_{1,1})$. Accordingly, the intensity-intensity correlation Eq. (19) exhibits second-order interference fringes, a manifestation of the so-called HBT effect.

From Eq. (19), it follows that the visibility of the interference fringes, defined by

$$\mathcal{V} = \frac{\max(N_{\text{coincidence}}) - \min(N_{\text{coincidence}})}{\max(N_{\text{coincidence}}) + \min(N_{\text{coincidence}})}, \quad (20)$$

cannot exceed 50%. It seems commonly accepted that the visibility of a two-photon interference experiment exceeding 50% is a criterion of the nonclassical nature of light. On the other hand, according to Ref.⁴³ the existence of high-visibility interference in the third and higher orders in the intensity cannot be considered as a signature of three- or four-photon interference. Thus, it seems that the two-photon case may be somewhat special, although there is no solid argument why this should be so.

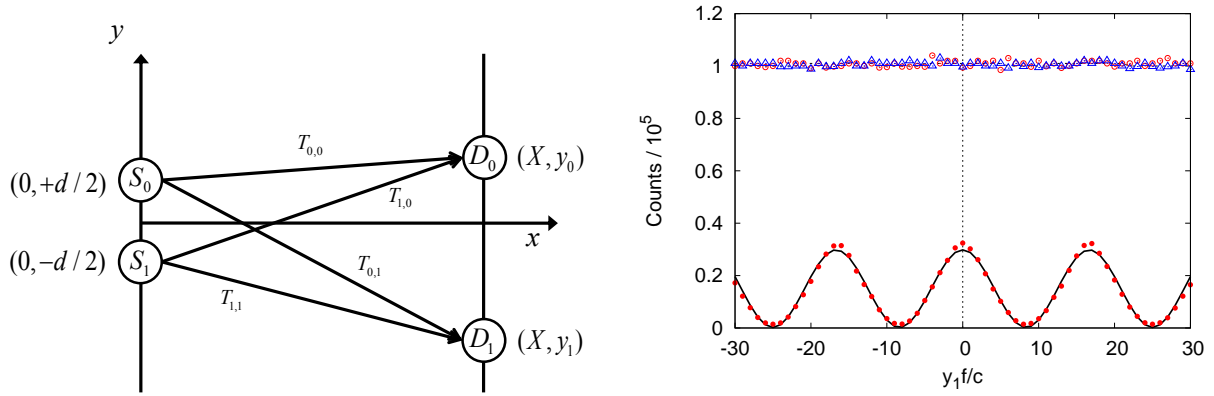


Figure 5. Schematic diagram of a HBT experiment. Left: Single photons emitted from point sources S_0 and S_1 are registered by two detectors D_0 and D_1 . The time-of-flight for each of the four possible paths from source S_m to detector D_n is denoted by $T_{m,n}$ where $m, n = 0, 1$. Right: Computer simulation data of the single-particle and two-particle counts for the HBT experiment depicted in Fig. 5. Red open circles: EBCM results for the counts of detector D_0 . Blue open triangles: EBCM results for the counts of detector D_1 . Red closed circles: EBCM results for the coincidence counts. The dashed and solid lines are least-square fits of the predictions of wave theory to the EBCM data for the single detector and coincidence counts, respectively. Simulation parameters: $N_{\text{tot}} = 2 \times 10^5$ events per $y_1 f/c$ -value, $N_F = 40$, $X = 100000c/f$, $d = 2000c/f$, $\gamma = \hat{\gamma} = 0.99$, $N_p = 2$, $W = 2/f$, $T_{\text{max}} = 2000/f$ and $h = 8$.

HBT experiments that detect the arrival of single particles employ time-coincidence to measure the intensity-intensity correlations. It is therefore quite natural to expect that a model that purports to explain the observations should account for the time delay that occurs between the time of arrival at a detector and the actual click of that detector. In quantum theory, time is not an observable and can therefore not be computed within the theory proper, hence there is no way that these time delays, which are being measured, can be accounted for by quantum theory. Consequently, any phenomenon that depends on these time delays must find an explanation outside the realm of quantum theory (as it is formulated to date).

7.1 EBCM model

For simplicity, we fix detector D_1 at $(X, 0)$ and study the single detectors and coincidence counts as a function of the y -position of detector D_0 . According to the general scheme, in each simulation step, both sources S_0 and S_1 create a messenger with their initial time-of-flight set to some randomly chosen messages \mathbf{y}_m ($m = 0, 1$) which are kept fixed for N_F successive pairs of messengers. Two pseudo-random numbers are used to determine whether the messengers travel to detector D_0 or D_1 . The time-of-flights are given by

$$T_{m,n} = \frac{\sqrt{X^2 + ((1-2m)d/2 - y_n)^2}}{c}, \quad (21)$$

where $m = 0, 1$ and $n = 0, 1$ label the source and detector, respectively. Averaging over the randomness in the initial messages wipes out all interference fringes in the single-detector counts, in agreement with Maxwell's theory.²⁵ Denoting the total number of emitted pairs of messengers by N_{tot} , we find that the number of single-detector counts fluctuates around $N_{\text{tot}}/2$, as expected from Maxwell's theory, providing numerical evidence that the detectors have indeed 100% detection efficiency. Similarly, the data for the coincidence counts (not shown) are in excellent agreement with the expression

$$N_{\text{coincidence}} = \frac{N_{\text{tot}}}{8} \left(1 + \frac{1}{2} \cos 2\pi f \Delta T \right), \quad (22)$$

predicted by Maxwell's theory (see Eq. (19)).

It is now straightforward to add a time-delay mechanism to the EBCM of the detector. We assume that the time at which the detector clicks, relative to the time of emission, is given by

$$t_{\text{delay}} = T_{m,n} + rT_{\text{max}}(1 - |\mathbf{T}|^2)^h, \quad (23)$$

where $0 < r < 1$ is a pseudo-random number, and \mathbf{T} is given by Eq. (4). The time scale T_{max} and the exponent h are free parameters of the time-delay model. Coincidences are counted by comparing the difference between the delay times of detectors D_0 and D_1 with a time window W , exactly in the same way as is done in the EPRB experiment (see Eq. (13)).

From the simulation results presented in Fig. 5, it is clear that by taking into account that there are fluctuations in the time delay that depend on the time-of-flight and the internal state of the detector, the visibility changes from $\mathcal{V} = 50\%$ to $\mathcal{V} \approx 100\%$. In Fig. 5, the solid line represents the least square fit of $a(1 + b \cos 2\pi f \Delta t)$ to the simulation data.

This example demonstrates that a purely classical corpuscular model of a two-photon interference experiment can yield visibilities that are close to 100%, completing the picture that high visibilities in two-, three- or four-photon interference experiments can be explained within the realm of a classical theory, such as an EBCM. In any case, the commonly accepted criterion of the nonclassical nature of light needs to be revised.

For simplicity, we have confined our presentation to the case of a definite polarization. Simulations with randomly varying polarization (results not shown) are also in concert with Maxwell's theory. Elsewhere, we have shown that three-photon interference can be modeled by an EBCM as well.²² The time delay model Eq. (23) is perhaps one of the simplest that yields interesting results but it is by no means unique.

8. SUMMARY AND OUTLOOK

We have demonstrated that one universal event-based corpuscular model (EBCM) for the interaction of photons with matter suffices to explain the interference and correlation phenomena that are observed when individual photons are detected one by one. Of course, this model produces the frequency distributions for observing many photons that are in full agreement with the predictions of Maxwell's theory and quantum theory. This is not surprising: Maxwell's theory is used as a guiding principle to determine the single-event dynamics of the model. The main conclusion of these simulations is that the effects such as EPR correlations and enhanced visibility in two-photon interference in the HBT experiment are contained in a corpuscular model of light and simply appear as the result of the particular processing of the detection events. The EBCM is entirely classical in the sense that it uses concepts of the macroscopic world and makes no reference to quantum theory but is nonclassical in the sense that it does not rely on the rules of classical Newtonian dynamics.

From its construction, it is clear the EBCM is contextual and produces events with frequency distributions that agree with the probabilistic predictions of quantum theory. The fact that the EBCM reproduces, for instance, the correlations of the singlet state without violating Einstein's local causality criterion suggests that the the date generated by the EBCM cannot be represented by a single Kolmogorov probability space. This complies with the idea that contextual, non-Kolmogorov models can lead to to violations of Bell's inequality without appealing to nonlocality or nonobjectivity.^{44, 45}

An important question is whether the EBCM can make predictions that can be tested experimentally. From the examples presented in this work, it is clear that after a few hundreds of photons have been processed by the EBCM, the frequencies of observations are hardly distinguishable from the intensities expected from Maxwell's theory (recall that the EBCM of the detector has 100% detection efficiency). Therefore, to test the EBCM, one has to conceive an experiment that is capable of testing the transient regime of the EBCM, that is the regime before the EBCM reaches its stationary state. Elsewhere we have proposed an experiment with a Mach-Zehnder interferometer that might be used for this purpose.²⁷ We hope that our simulation results will stimulate the design of new time-resolved single-photon experiments to test our corpuscular model for optical phenomena.

We would like to draw attention to the fact that the EBCM approach may have practical applications as a new method for simulating optical phenomena. Indeed, the work presented in this paper may open a route to rigorously include the effects of interference in ray-tracing software. For this purpose, it may be necessary to

extend the DLM-based model for a lossless dielectric material to, say a Lorentz model for the response of material to the electromagnetic field⁴⁶ and to extend the model to simulate phenomena that, in Maxwell's theory, are due to evanescent waves. We leave these extensions for future research.

9. ACKNOWLEDGEMENT

We would like to thank K. De Raedt and S. Miyashita for many helpful comments. This work is partially supported by NCF, the Netherlands.

REFERENCES

- [1] Grangier, P., Roger, G., and Aspect, A., "Experimental evidence for a photon anticorrelation effect on a beam splitter: A new light on single-photon interferences," *Europhys. Lett.* **1**, 173 (1986).
- [2] Jacques, V., Wu, E., Toury, T., Treussart, F., Aspect, A., Grangier, P., and Roch, J.-F., "Single-photon wavefront-splitting interference – An illustration of the light quantum in action," *Eur. Phys. J. D* **35**, 561–565 (2005).
- [3] Merli, P. G., Missiroli, G. F., and Pozzi, G., "On the statistical aspect of electron interference phenomena," *Am. J. Phys.* **44**, 306–307 (1976).
- [4] Tonomura, A., Endo, J., Matsuda, T., Kawasaki, T., and Ezawa, H., "Demonstration of single-electron buildup of an interference pattern," *Am. J. Phys.* **57**, 117–120 (1989).
- [5] Tonomura, A., [*The Quantum World Unveiled by Electron Waves*], World Scientific, Singapore (1998).
- [6] Rauch, H., Treimer, W., and Bonse, U., "Test of a single crystal neutron interferometer," *Physics Letters A* **47**(5), 369 – 371 (1974).
- [7] Rauch, H. and Werner, S. A., [*Neutron Interferometry: Lessons in Experimental Quantum Mechanics*], Oxford Univ. Press, London (2000).
- [8] Rauch, H. and Summhammer, J., "Static versus time-dependent absorption in neutron interferometry," *Phys. Lett. A* **104A**, 44 – 46 (1984).
- [9] Roychoudhuri, C., "Principle of non-interaction of waves," *J. Nanophotonics* **4**, 043512 (2010).
- [10] Roychoudhuri, C., "Measurement Epistemology and Time-Frequency Conjugate Spaces," in [*Quantum Theory: Reconsideration of Foundations - 5*], Khrennikov, A., ed., **1232**, 143 – 152, AIP Conference Proceedings, Melville and New York (2010).
- [11] De Raedt, H., De Raedt, K., and Michielsen, K., "Event-based simulation of single-photon beam splitters and Mach-Zehnder interferometers," *Europhys. Lett.* **69**, 861 – 867 (2005).
- [12] De Raedt, K., De Raedt, H., and Michielsen, K., "Deterministic event-based simulation of quantum interference," *Comp. Phys. Comm.* **171**, 19 – 39 (2005).
- [13] De Raedt, H., De Raedt, K., and Michielsen, K., "New method to simulate quantum interference using deterministic processes and application to event-based simulation of quantum computation," *J. Phys. Soc. Jpn. Suppl.* **76**, 16 – 25 (2005).
- [14] Michielsen, K., De Raedt, K., and De Raedt, H., "Simulation of Quantum Computation: A Deterministic Event-Based Approach," *J. Comput. Theor. Nanosci.* **2**, 227 – 239 (2005).
- [15] De Raedt, K., Keimpema, K., De Raedt, H., Michielsen, K., and Miyashita, S., "A local realist model for correlations of the singlet state," *Euro. Phys. J. B* **53**, 139 – 142 (2006).
- [16] De Raedt, H., De Raedt, K., Michielsen, K., Keimpema, K., and Miyashita, S., "Event-based computer simulation model of Aspect-type experiments strictly satisfying Einstein's locality conditions," *J. Phys. Soc. Jpn.* **76**, 104005 (2007).
- [17] De Raedt, K., De Raedt, H., and Michielsen, K., "A computer program to simulate Einstein-Podolsky-Rosen-Bohm experiment with photons," *Comp. Phys. Comm.* **176**, 642 – 651 (2007).
- [18] De Raedt, H., De Raedt, K., Michielsen, K., Keimpema, K., and Miyashita, S., "Event-by-event simulation of quantum phenomena: Application to Einstein-Podolsky-Rosen-Bohm experiments," *J. Comp. Theor. Nanosci.* **4**, 957 – 991 (2007).
- [19] Zhao, S., De Raedt, H., and Michielsen, K., "Event-by-event simulation model of Einstein-Podolsky-Rosen-Bohm experiments," *Found. of Phys.* **38**, 322 – 347 (2008).

- [20] Zhao, S. and De Raedt, H., “Event-by-event Simulation of Quantum Cryptography Protocols,” *J. Comp. Theor. Nanosci.* **5**, 490 – 504 (2008).
- [21] Zhao, S., Yuan, S., De Raedt, H., and Michielsen, K., “Computer simulation of Wheeler’s delayed choice experiment with photons,” *Europhys. Lett.* **82**, 40004 (2008).
- [22] Jin, F., De Raedt, H., and Michielsen, K., “Event-by-event simulation of the Hanbury Brown-Twiss experiment with coherent light,” *Commun. Comput. Phys.* **7**, 813 – 830 (2010).
- [23] Jin, F., Yuan, S., De Raedt, H., Michielsen, K., and Miyashita, S., “Particle-only model of two-beam interference and double-slit experiments with single photons,” *J. Phys. Soc. Jpn.* **79**, 074401 (2010).
- [24] Jin, F., Zhao, S., Yuan, S., De Raedt, H., and Michielsen, K., “Event-by-event simulation of a quantum eraser experiment,” *J. Comp. Theor. Nanosci.* **7**, 1771–1782 (2010).
- [25] Michielsen, K., Jin, F., and De Raedt, H., “Event-based Corpuscular Model for Quantum Optics Experiments,” *J. Comp. Theor. Nanosci.* **8**, 1052 – 1080 (2011).
- [26] Born, M. and Wolf, E., [*Principles of Optics*], Pergamon, Oxford (1964).
- [27] Michielsen, K., Richter, M., Lippert, T., Barbara, B., Miyashita, S., and De Raedt, H., “Proposal for an interference experiment to test the applicability of quantum theory to event-based processes,” *submitted to New J. Phys.* (2010). <http://arxiv.org/abs/1006.0174>.
- [28] Garrison, J. C. and Chiao, R. Y., [*Quantum Optics*], Oxford University Press, Oxford (2009).
- [29] Hadfield, R. H., “Single-photon detectors for optical quantum information applications,” *Nature Photonics* **3**, 696 – 705 (2009).
- [30] Ballentine, L. E., [*Quantum Mechanics: A Modern Development*], World Scientific, Singapore (2003).
- [31] Home, D., [*Conceptual Foundations of Quantum Physics*], Plenum Press, New York (1997).
- [32] Trieu, B., Michielsen, K., and De Raedt, H., “Event-based simulation of light propagation in lossless dielectric media,” *Comp. Phys. Comm.* **182**, 726–734 (2011).
- [33] Wheeler, J. A. (1983). in: *Mathematical foundations of quantum theory*, Proc. New Orleans Conf. on The mathematical foundations of quantum theory, ed. A.R. Marlow (Academic, New York, 1978) [reprinted in *Quantum theory and measurements*, eds. J.A. Wheeler and W.H. Zurek (Princeton Univ. Press, Princeton, NJ, 1983) pp. 182-213].
- [34] Jacques, V., Wu, E., Grosshans, F., Treussart, F., Grangier, P., Aspect, A., and Roch, J.-F., “Experimental Realization of Wheeler’s Delayed-Choice Gedanken Experiment,” *Science* **315**, 966–968 (2007).
- [35] Jacques, V., Wu, E., Grosshans, F., Treussart, F., Grangier, P., Aspect, A., and Roch, J.-F., “Delayed-Choice Test of Quantum Complementarity with Interfering Single Photons,” *Phys. Rev. Lett.* **100**, 220402 (2008).
- [36] Weihs, G., Jennewein, T., Simon, C., Weinfurter, H., and Zeilinger, A., “Violation of Bell’s Inequality under Strict Einstein Locality Conditions,” *Phys. Rev. Lett.* **81**, 5039 – 5043 (1998).
- [37] Fine, A., “Some Local Models for Correlation Experiments,” *Synthese* **50**, 279 – 294 (1982).
- [38] Pascasio, S., “Time and Bell-type Inequalities,” *Phys. Lett. A* **118**, 47 – 53 (1986).
- [39] Brown, R. H. and Twiss, R. Q., “A Test of a New Type of Stellar Interferometer on Sirius,” *Nature* **178**, 1046–1048 (1956).
- [40] Glauber, R. J., “Photon correlations,” *Phys. Rev. Lett.* **10**, 84 – 86 (1963).
- [41] Glauber, R. J., “The quantum theory of optical coherence,” *Phys. Rev.* **130**, 2529 – 2539 (1963).
- [42] Mandel, L., “Quantum effects in one-photon and two-photon interference,” *Rev. Mod. Phys.* **71**, S274 – S282 (1999).
- [43] Agafonov, I. N., Chekhova, M. V., Iskhakov, T. S., and Penin, A. N., “High-visibility multiphoton interference of Hanbury Brown-Twiss type for classical light,” *Phys. Rev. A* **77**, 053801 (2008).
- [44] Khrennikov, A. Y., [*Contextual Approach to Quantum Formalism*], Springer, Berlin (2009).
- [45] Khrennikov, A., “On the role of probabilistic models in quantum physics: Bell’s inequality and probabilistic incompatibility,” *J. Comp. Theor. Nanosci.* **8**, 1006–1010 (2011).
- [46] Taflove, A. and Hagness, S., [*Computational Electrodynamics: The Finite-Difference Time-Domain Method*], Artech House, Boston (2005).